Available online at www.sciencedirect.com
ScienceDirect
Renewable Energy 32 (2007) 216–234
RENEWABLE ENERGY
www.elsevier.com/locate/renene

Effects of large-scale photovoltaic power integration on electricity distribution networks

Jukka V. Paatero*, Peter D. Lund

Advanced Energy Systems, Helsinki University of Technology, P.O. Box 2200, FI-02015 HUT, Finland

Received 3 September 2005; accepted 22 January 2006
Available online 22 March 2006

Abstract

The public support in photovoltaic (PV) technologies and increasing markets have resulted in extensive applications of grid-connected PV, in particular in the consumer side and electricity distribution grid. In this paper, the effects of a high level of grid connected PV in the middle voltage distribution network have been analyzed. The emphasis is put on static phenomena, including voltage drop, network losses and grid benefits. A multi-purpose modeling tool is used for PV analysis in Lisbon and Helsinki climates. All network types studied can handle PV without problems with an amount of PV equaling at least up to the load (1 kW_p/household). The comb-type network showed the best performance. The PV is unable to shave the domestic load peak in the early evening hours but through orientating the PV panels both to east and west, the noon peak from PV can be reduced by 30%. PV integration reduces network losses positively up to a 1 kW_p/hh (100% of annual domestic load) level. For 2 kW_p/hh all but the comb-type networks demonstrate clear over-voltage situations and the annual network losses are much higher than without PV.

Keywords: Photovoltaics; Network effects; Distributed power generation; Simulation

1. Introduction

Photovoltaic (PV) power generation has been steadily growing supported by large deployment campaigns in some countries [1]. Most of the new PV capacity is assigned to

*Corresponding author. Tel.: +358 9 451 32 13; fax: +358 9 451 31 95.
E-mail address: jukka.paatero@hut.fi (J.V. Paatero).

0960-1481/$ - see front matter © 2006 Elsevier Ltd. All rights reserved.
doi:10.1016/j.renene.2006.01.005

Nomenclature

A	type of appliance or group of appliances
A_c	total photovoltaic array area
d	day of the week
f	mean daily starting frequency, models the mean frequency of use for an appliance
h	hour of the day
hh	household
H	Jacobian matrix where $H_{ki} = \partial P_k / \partial \delta_i$
i	node index, used as subscript
I	incident solar insolation
$\mathbf{j}$	vector of current values
$\hat{j}$	complex unit
J	current in a line or node
k	node index, used as subscript
kW_p	power of photovoltaic unit by peak performance rating
L	Jacobian matrix where $L_{ij} = \partial Q_i / \partial U_j$
M	Jacobian matrix where $M_{ki} = \partial Q_i / \partial \delta_j$
n	number of network nodes
N	Jacobian matrix where $N_{ki} = \partial P_k / \partial U_i$
p_{season}	seasonal probability factor describing the season dependent changes
p_{hour}	hourly probability factor describing the activity levels during the day
p_{step}	scaling factor, scales the probabilities in relation to the time step used Δt comp
p_{social}	social random factor, models behavior influenced by weather and social factors
P	power through a node
P_{PV}	power a photovoltaic panel/system generates
Q	reactive power through a node
RN	random number
S	power loss on a network line
t	time index, used as subscript or superscript
t_{comp}	computational time
$\mathbf{u}$	vector of voltage values
U	voltage at a node
w	week of the year
Y	conductance of a line
Y_0	self inductance of a network node
Y'	matrix element of conductance matrix $\mathbf{Y}$. If $k \neq i$, then $Y'_{ki} = -Y_{ki}$, else $Y'_{kk} = Y_{k0} + \Sigma_{k=1,k\neq i}^{n} Y_{ki}$
$\mathbf{Y}$	matrix of inductance values
Z	impedance of a line

Greek letters

α	solar panel azimuth angle
δ	voltage phase angle at a node
Δ	a step in a variable (difference)
ε	convergence limit of an iteration
η	system conversion efficiency of the photovoltaic system
η_0	solar module efficiency
η_{inv}	photovoltaic system DC to AC conversion efficiency including losses in cablings
σ_{flat}	standard deviation for P_{social}

grid connected distributed power generation [2]. This raises new engineering challenges at individual household (hh) level due to the intermittency of the solar resource.

Advances in PV technology have been fast in recent years making this technology technically viable for local power production in small scale although the cost-effectiveness is not yet adequate. The state of art and prospects of PV technology have recently been reviewed by Green [3] and van der Zwaan [4]. The planning tools of individual photovoltaic systems are also well available for evaluating sizing and system economy [5,6].

When large-scale applications of PV in the grid are considered little references are, however, found on PV in the individual customer line. Most of the work on large-scale PV is reported either on large scale PV power generation in general e.g. in scenarios or on central PV power schemes [7]. Some experimental facilities on central PV power stations were erected already in the 1980s [8].

In the present paper, large-scale implementation of distributed photovoltaic power generation in the end-use side is studied. The individual PV systems are scattered into the consumer nodes and connected to the distribution network. We have used a distribution network simulation tool to provide over 150 different case studies to get a detailed view of the effects from high photovoltaic penetration. These case studies include two geographical locations with a total of three different domestic electricity consumption profiles that were created using a load method published earlier by the authors [9]. Five different penetration levels and four different strategies for orientating the solar panels were included. The main parameters used for evaluating the impacts of PV on the distribution network are the voltage balance, system losses, and peak load compensation. Our results show, that the medium voltage distribution network can be straightforwardly modeled to evaluate the effects of high PV penetration levels.

2. Methodology

The power distribution system in this paper is modeled with the DESIGEN simulation tool (decentralized system simulation tool for optimized generation) developed at Helsinki University of Technology. Fig. 1 shows the flow chart of DESIGEN and the iterative processes used to solve the power flows and balances. The program combines power flow calculations, custom load data and models for distributed power generation and simulates the static power flow effects with a given time interval, usually using an 1 h time step.

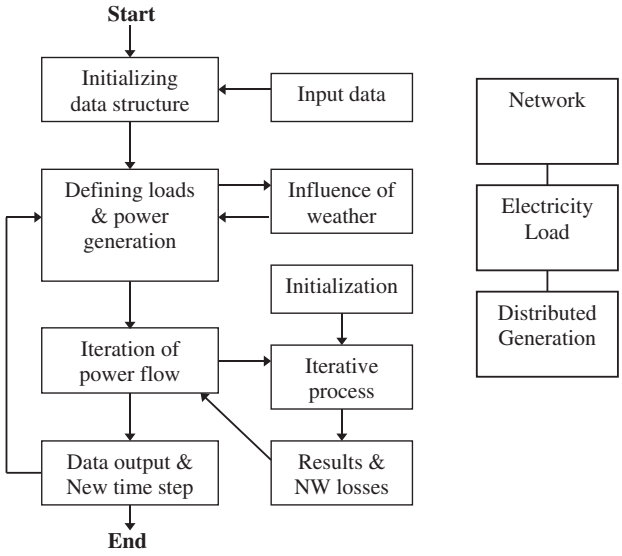

Fig. 1. Structure of DESIGEN simulation tool. Left: flow diagram for the computational structure. Right: main elements of the program.

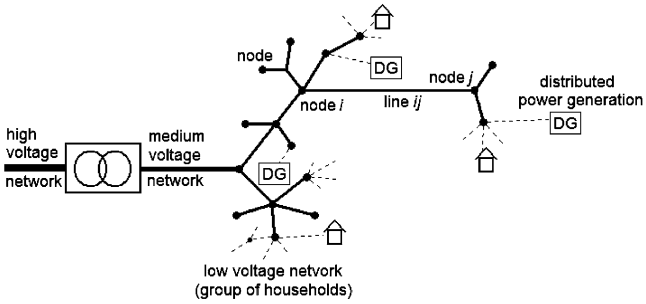

Fig. 2. Schematic illustration of a distributed energy system with network, load and generation units.

To compare the system performance in a temperate and cold climate, the load and PV generation data included two climatic zones: Helsinki (60°N) and Lisbon (39°N).

The type of energy system modeled is sketched in Fig. 2 showing a hypothetical network, loads and distributed generation units. In the simulation runs, the PV systems are distributed evenly, i.e. each node in the network includes PV. As the low voltage network is not simulated per se, one medium voltage node represents typically a group of houses, or about 40 hhs each.

2.1. Power distribution network

DESIGEN employs two different network calculation methods. The first one calculates radial networks using a simple five step iterative method similar to that published by Jenkins et al. [10]. The method is described in detail in Appendix A.

The second network calculation method solves looped networks using the traditional polar power-mismatch version of the iterative Newton–Raphson algorithm [11,12], designed for solving a set of non-linear equations simultaneously. There, network flow equations form a so-called Jacobian-matrix equation

$$\begin{bmatrix} \Delta P_t \\ \Delta Q_t \end{bmatrix} = \begin{bmatrix} H & N \\ M & L \end{bmatrix} \begin{bmatrix} \Delta \delta_t \\ \Delta U_t \end{bmatrix}, \tag{1}$$

which is iteratively solved until the power values $P_{t+1} = P_t + \Delta P_t$ (real power) and $Q_{t+1} = Q_t + \Delta Q_t$ (reactive power) converge. The matrixes H, N, M and L above are Jacobian matrixes $H_{ki} = \partial P_k/\partial \delta_i$, $N_{ki} = \partial P_k/\partial U_i$, $M_{ki} = \partial Q_k/\partial \delta_i$ and $L_{ki} = \partial Q_k/\partial U_i$, correspondingly. $\Delta \delta_t$ is the phase angle and ΔU_t the voltage step size. This traditional Newton–Raphson method was chosen due to its simplicity, although faster decoupled power flow method exists [13,14]. The modeled network can include transformers and all kinds of load and generation components, including reactive current compensators. The whole procedure for simulating looped networks is available in Appendix B.

The transmission losses of both the radial and looped networks can be calculated for each time step as

$$S_{ki} = (U_k - U_i)J_{ki}^* = Y_{ki}^*[U_k - U_i]^2, \tag{2}$$

where loss S_{ki} on line between adjacent nodes k and i is computed using voltage U_k for node k and U_i for node i, correspondingly. Y_{ki} is the admittance between the nodes i and k. J_{ki} is the current.

DESIGEN can also be applied to model transformers in the network, but it is out of the scope here, as only one distribution network level is considered.

2.2. Consumer load

DESIGEN reads the end-use load for each network node in the power distribution network from a file. In practice, the load data is simulated separately using a statistical approach to handle a large load data set.

The load model is described in detail elsewhere [9]. The key input data needed include firstly the mean electricity consumption rate and the season induced weekly changes in mean load on an annual level. Secondly, the appliances to be included into the model and their mean daily consumption profiles, preferably separately for weekdays and weekend days, need to be defined. Next the cycle length, power levels and standby power level of each appliance type used need to be defined. Reactive power can also be included. Finally, the mean saturation levels per hh and average usage per day of the appliances is defined.

Based on the above data and statistics, hourly load profiles are created stochastically for each consumer node individually. For each time point the usage (on/off) of the appliances is determined. The turning-on criterion of an appliance is checked with a random number RN (0,1) using the following criterion:

$$\begin{aligned} &\text{IF RN} \leqslant P_{\text{start}} \text{ the appliance is ON, ELSE appliance is OFF} \\ &P_{\text{start}}(A, w, \Delta t_{\text{comp}}, \sigma_{\text{flat}}, h, d) \\ &= P_{\text{season}}(A, w)P_{\text{hour}}(A, h, d)f(A, d)P_{\text{step}}(\Delta t_{\text{comp}})P_{\text{social}}(\sigma_{\text{flat}}), \end{aligned} \tag{3}$$

where P_{season} is the seasonal probability factor describing the season dependent changes, P_{hour} the hourly probability factor describing the activity levels during the day, P_{step} the scaling factor, scales the probabilities in relation to the time step used Δt_{comp}, P_{social} the social random factor, models behavior influenced by weather and social factors, f the mean daily starting frequency, models the mean frequency of use for an appliance [1/day], A the type of appliance or group of appliances, h the hour of the day, d the day of the week, w the week of the year, Δt_{comp} the computational time step [here 60 min], σ_{flat} the standard deviation for P_{social}.

The procedure described results in a consumption pattern with a realistic statistical behavior [9].

2.3. Power generation models

In addition to customer loads, distributed generation technologies can be included into the distribution network modeled by DESIGEN. The power generation units form their own nodes in the distribution network for modeling reasons. In present paper only local PV generation is described, but the DESIGEN includes also other technology options.

For the PV modules, a temperature dependent PV model has been applied. The output from the photovoltaic array P_{PV} is calculated as follows:

$$P_{PV} = A_c \times I \times \eta, \tag{4}$$

where A_c is the total array area, I the incident solar insolation, and η the system conversion efficiency of the photovoltaic system. The solar radiation on the PV surface is calculated using standard incidence angle formulas [15]. The time step for the calculation is 1 h.

The system efficiency η is composed mainly of three factors: the solar module efficiency (η_0) and its temperature dependence and the DC to AC conversion efficiency (η_{inv}) including losses in cablings. This can be presented for silicon solar cells in the following way:

$$\eta = \eta_0 \times \left[1 - 0.0042 \times \left(\frac{I}{18} + T_a - 20\right)\right] \times \eta_{inv}, \tag{5}$$

where T_a is the ambient temperature. Typically $\eta_{inv} = 0.85$ and $\eta_0 = 0.15$. The temperature dependence of the solar module conversion efficiency is described by the correlation inside the brackets and it may influence the efficiency by tens of percents. PV temperature elevation reduces the solar electricity conversion efficiency typically by 0.4–0.5%/C°.

To account for possible obstructions or shadings at low solar elevation in urban environments, Eq. (4) is subject to a threshold value, or $P_{PV} = 0$ if $I < 50\,W/m^2$.

3. Input data

The aim of the case studies is to determine the weak and critical points in the middle voltage distribution network when a large amount of PV power generation is integrated into the network. A total of 153 case studies was analyzed to high-light these issues. The input data sets comprised the following:

- 3 sets of hh load profiles in 2 climates, 2 in Portugal and 1 in Finland;
- 2 radial and 1 looped network setups;

- 4 climate specific orientation strategies of the PV panels;
- 4 four different penetration levels of PV power generation.

This yields $3 \times 3 \times 4 \times 4 = 144$ cases to be simulated by DESIGEN. 9 reference case studies without PV panels were also included which yields then a total of 153 simulations.

3.1. Network setups

The first network geometry studied in the medium voltage distribution network setups is a multi-branched tree-type network, which corresponds mainly to an urban distribution network. Due to its symmetrical shape, some of the branches were reduced to one node in order to improve computational speed. The final network includes 118 nodal points with a total of 9840 hhs, including one high voltage supply double node, shown as node 1 in Fig. 3a. About 40% of the network was reduced due to symmetry as shown in Fig. 3a. Nodes number 23, 26 and 93 represent the reduced symmetrical network branches through a single node representing each a 33 node branch. Some minor reductions in less significant parts of network have been made, namely nodes 22, 24, 25, 27, 91 and 93, respectively. The numbers followed by a small "*k*" indicate the number of hhs in the reduced branches.

The shape of the second network is a comb-type network with two linear and symmetrical branches with a short side branch in-between. The network has a high voltage feeding node in one end of the branches (node number 1). This geometry includes a particularly strong main line and weak side branches. The network includes a total of 236 nodal points and 9360 hhs. Due to symmetry only 50% of the network needs to be computed. Fig. 3b shows the computational network excluding the symmetrical branch.

The third network is shaped as two opposite loops resembling number eight. The loops have short side branches. The looped form allows the main line to be triple the length of the linear network using weaker main line cables. Also, due to the loops the network was made of a simplified structure that allows faster computation. This network includes a total of 113 nodal points and 8960 hhs, while only 50% of the network needed to be computed. Fig. 3c shows the computational network excluding the symmetrical branch.

The networks shown in Fig. 3 employ cable types presented in Table 1. The tree-network uses Ibis-type cables between node 1 and nodes 4, 14 and 82. The thicker branches (main cables) are Raven-type while the rest are Sparrow-type. In the loop-network the main loop is Ibis-type while the side branches are Sparrow-type. The Condor-type cable is used only in the comb-network, where it goes from nodes 1 to 104 while the side branches are Ibis-type and the sub branches Raven-type.

The voltage of the network should preferably stay within 0.975 and 1.025 p.u. when PV is connected. These limits were chosen as a compromise when the rural (5–15% of nominal voltage) and urban (0.5–2%) voltage drop recommendations given by ABB were considered [16]. The unit p.u. stands for Per Unit which corresponds to the voltage relative to the nominal value which is 20 kV in the medium voltage network used here. The described choice of network cables was necessary to achieve a minimum voltage of 0.975 p.u. in each network with all the different load sets. An additional limit to the network was the feeding node that was limited to a voltage 1.0 p.u. in order to accommodate the PV integration. As a result, the comb-type network became very strong, able to handle some 10,000 hhs. As strongest network it would be least effected by the PV integration shown later in the analysis chapter.

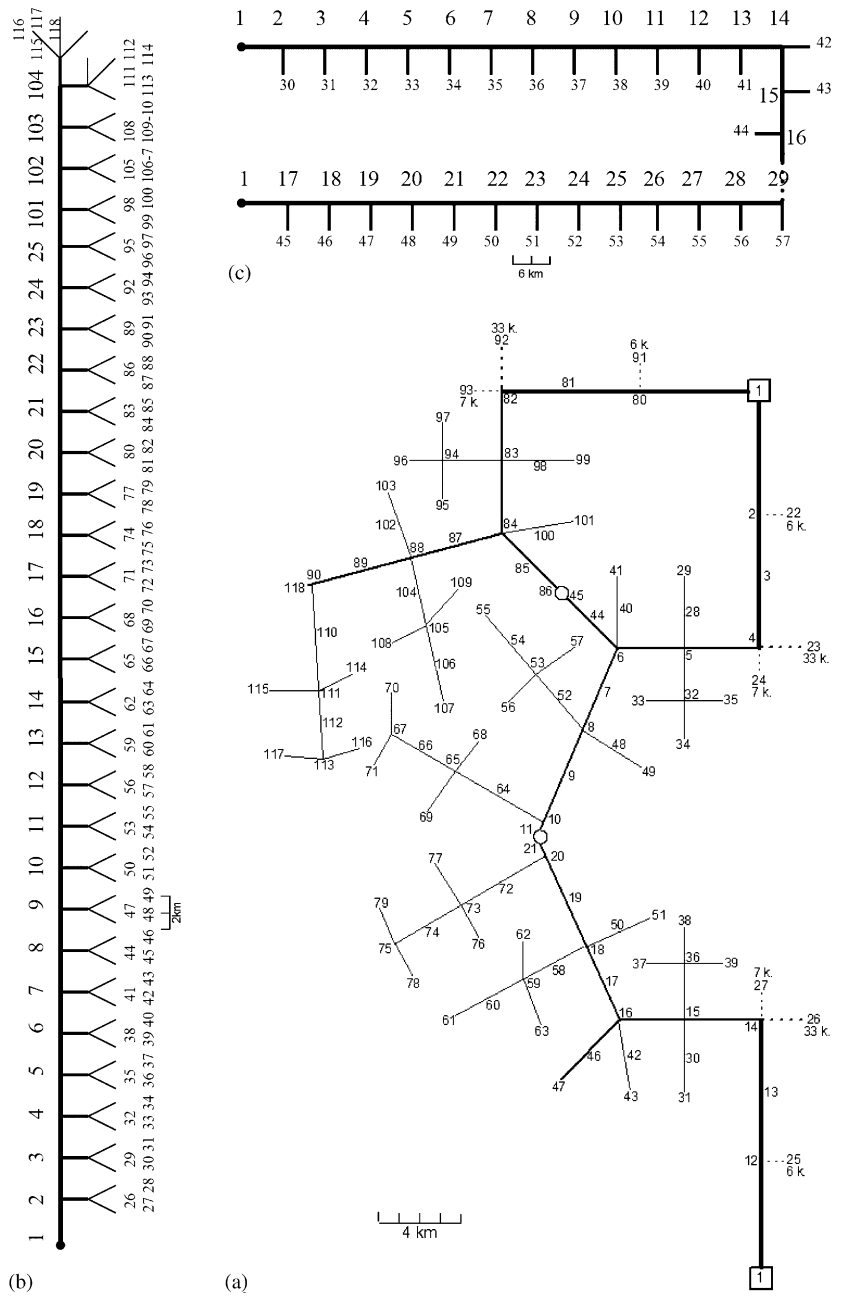

Fig. 3. Network topologies used in reduced form. Numbers in figures correspond to the nodes: (a) Tree-type network, where some of the symmetrical or unimportant network branches have been reduced to single node. Letter '*k*' next to the node indicates the number of end nodes in the reduced branch. (b) Loop-type network. Two such branches are used in the simulation. Node 1 has been showed in double for the sake of clarity. (c) Comb-type network. Two such branches are used in the simulation.

Table 1
Cable types used in the electrical networks

Cable name	Cross section (mm^2)	Cable resistance (Ω/km)	Inductive resistance (Ω/km)	Maximum power (MW)
Sparrow	33.8	0.849	0.377	4.2
Raven	53.5	0.537	0.358	5.6
Ibis	201	0.145	0.302	13.2
Condor	402	0.075	0.282	20.0

For all the three networks, a set of simulations were performed. As a reference, simulations with no PV power generation were first executed for each network and load set. This totaled nine runs, with three different load sets per network. The amounts of consumers have been selected in such a way, that the annual minimum of the hourly voltage is between 0.975 and 0.974 p.u. in normalized units which is an often used design limit.

3.2. Household load profiles

The Finnish hh data set applied in this work is based on the data presented in [9] and the Portuguese data sets were created by the same method. The data profiles are based on publicly available statistics and data. The load data represents apartment houses.

The first consumption profile is based on experimental data from Finnish blocs of flats. This data has been analyzed and modeled in Ref. [9]. In addition, the reactive consumption of hhs is also modeled here.

The second consumption profile is generated with the same model as above, but using domestic consumption data from Portugal and Lisbon in particular. Three data sources were mainly used there: the total domestic electricity consumption in Lisbon 2003 [17], estimated population data of the same year [18,19], and mean saturation levels for domestic appliances in Portugal [19–21]. The weekly annual load curve was compiled based on unpublished test reference year weather and insolation data from Lisbon, compiled in the same manner as the CEC 1985 data [22]. Public weather data from Lisbon is available at Russian Weather Archive [23]. As the annual changes in Lisbon weather are rather small, slightly convex consumption patterns were generated except cold appliances that follow a hump-like model presented in [19].

The third consumption profile is from most parts similar on the second one. The difference in this model is that 50% of the hhs are assumed to be air-conditioned based on the equipment profiles measured in Ref. [19].

The main characteristics of the three applied datasets are shown in Table 2. Daily mean loads over 1 year are shown in Fig. 4. The load profiles differ significantly in their shapes and magnitude as well as in the amount of reactive load. Very important for the PV applications is the shape of annual load curve and clearly the case of Lisbon with air conditioning provides a promising shape with a lot of summer time consumption. The mean hourly consumption is shown later in the Analysis chapter along with some results. In the Helsinki data set, the weekend and week day load curves are modeled separately.

Table 2
Key figures of the household data sets

Data set	Hki	Lbon	Lbon + AC	Units	Period
Mean annual energy	1859	2360	2527	kWh/hh	Jan–Dec
Mean winter months energy	514	568	578	kWh/hh	Dec–Feb
Mean summer months energy	409	625	716	kWh/hh	Jun–Aug
Annual maximum power	453	459	502	W/hh	19 Nov/19 Nov/24 Aug
Annual minimum power	98	140	145	W/hh	18 Jul/11 Apr/02 Apr
Annual maximum in reactive power	44	91	97	VAR/hh	13 Jan/12 Aug/29 Jul
Annual minimum in reactive power	35	43	44	VAR/hh	14 Jan/04 Mar/28 Jan

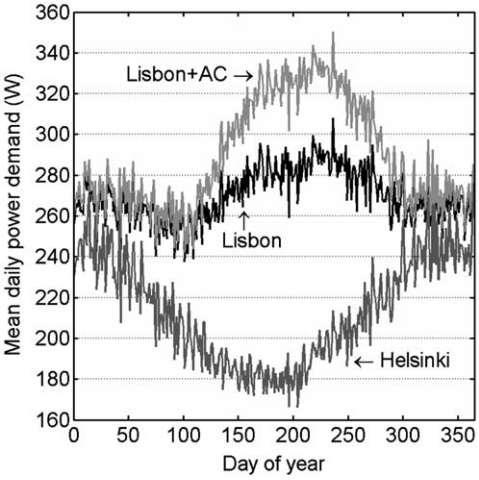

Fig. 4. Daily energy demand levels for the different household types on an annual level. 'Lisbon + AC' refers to the Lisbon load with air conditioning.

3.3. PV setups

The PV options considered included 4 different levels of penetration of PV in the network and 4 orientation cases of the panels. The orientation of the PV modules has an important effect on the temporal behavior of the PV output and on its matching with the load. The share of the PV of hh electricity was sized at 5%, 50%, 100% and 200% of hhs having a 1 kW_p PV system. The 200% corresponds to a 2 kWp PV capacity per each hh.

The inclination angle of the PV panels on the house roofs was chosen optimally for the two locations: 30° for Lisbon and 45° for Helsinki, respectively. The orientation of the panels was varied to cover different town planning cases as follows:

- all panels pointing to south (azimuth angle $\alpha = 0°$);
- 50% of the panels to south, 25% to east ($\alpha = -90°$) and 25% to west ($\alpha = 90°$);
- 50% of the panels to south and 50% to west;
- 50% of the panels to east and 50% to west.

4. Analysis

In the next, the results from the simulation runs using the above described input data sets are described in more detail.

4.1. Effect of climate and household types

The local climate affects mainly the total PV electricity produced through the available solar radiation. Thus, Helsinki representing a northern climate gives typically 50–60% less PV output than in Lisbon on an annual base. The Helsinki weather caused considerable fluctuation in PV output over time whereas the Lisbon was quite stable. This is well demonstrated in Fig. 5 for a summer week. The power peaks were of same magnitude in both climates and the maximum hourly PV output was found in early spring due to sunny but cool weather.

The hh load profiles also differ quite much. In Helsinki, the consumption peak is in the late autumn and a high consumption level continues through all the winter. On the other hand, the Lisbon consumption peak occurs at the end of July and beginning of August and most of the summer is high consumption season. This is found both with and without the air conditioning which only emphasizes the weight of summer consumption.

The summer peak found in Lisbon may suggest that PV could match ideally the consumption of electricity. Unfortunately, the main energy consumption takes place both in Lisbon and Helsinki in the evening. There is a 7–8 h difference between the PV and load peaks and the PV production in Lisbon is almost at zero when the evening peak begins. In Helsinki, the situation is slightly better as the evening peak is smoother and wider. The mean PV production in summer in Helsinki therefore cuts slightly the evening peak, but not the main peak to influence the low voltage levels during peak load hours. Mean

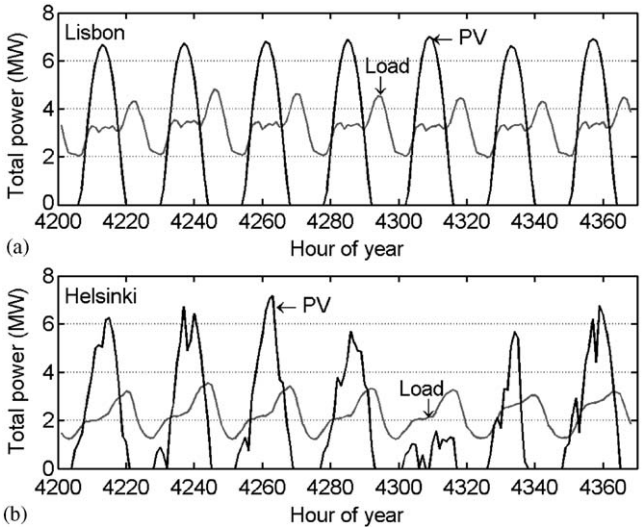

Fig. 5. Illustration of hourly summer-time load and PV power levels for (a) Lisbon and (b) Helsinki. The PV penetration level is 1 kW_p per household, azimuth angle is 0°.

summer and winter time PV production and consumption curves for both locations are shown in Fig. 6.

4.2. Effect of PV panel orientation

The 4 PV azimuth angle cases provided a good view how orientation could affect the load and PV matching. Fig. 7 illustrates the summer time average output for the different cases. The ''East–West''-case has the most flat mean power, but the total energy production is reduced. On the other hand, the ''All South''-case gives the highest total energy output as expected, but the shape of the PV curve is steepest of all cases. The ''South–West'' and ''South–East–West'' cases lie in between the two previous curves.

Fig. 8 illustrates the system dynamics on an hourly scale for different orientation cases in Helsinki and Lisbon during a clear summer day. The power generation peak during the PV operation is smoother when the PV panels are orientated to east and west than to the south only, or 10% smoother in Lisbon and 30% in Helsinki, respectively. Accordingly, network

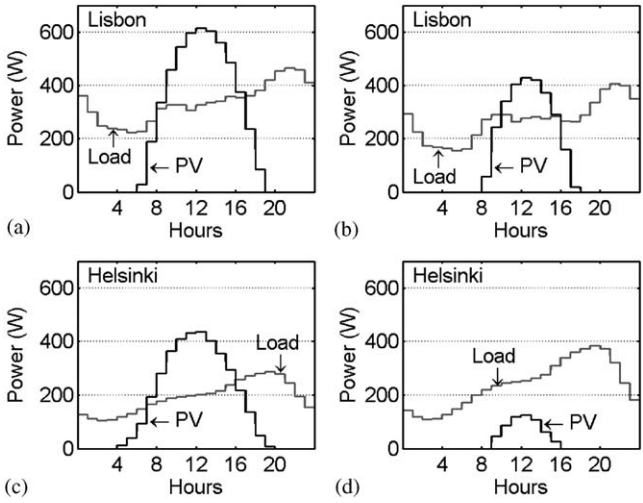

Fig. 6. Summer and winter mean consumption and PV generation: (a) Lisbon summer, (b) Lisbon winter, (c) Helsinki summer, (d) Helsinki winter. The PV penetration level is 1 kW_p per household, azimuth angle is 0°.

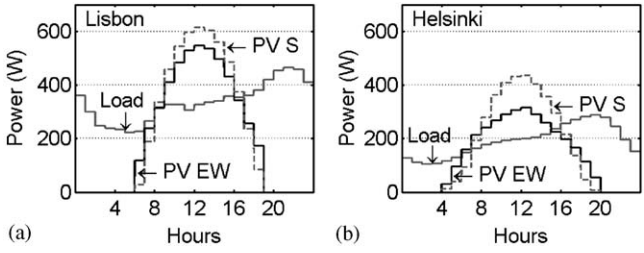

Fig. 7. Summer time mean consumption and PV generation. Fifty percent of the PV panels are orientated to the west and 50% to the east. (a) Lisbon summer, (b) Helsinki summer. Dotted line corresponds to all panels orientated to the south. The PV penetration level is 1 kW per household.

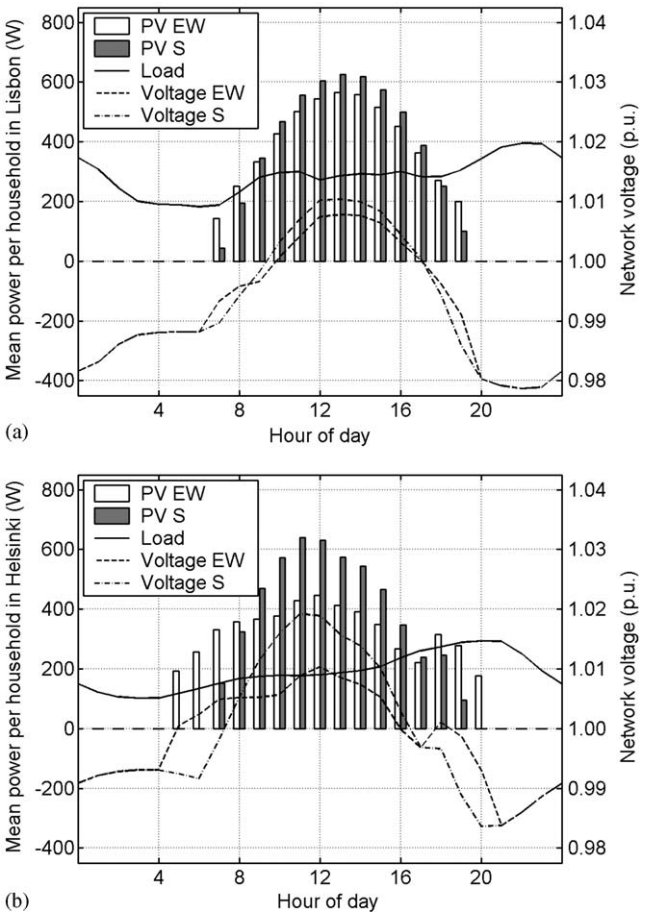

Fig. 8. Example of hourly dynamics of the distributed energy system with PV on a summer day.

over-voltage is reduced 25% in Lisbon and 46% in Helsinki. The total solar yields from the panels would not different much between the two cases for the day shown but on an annual bases the East–West case would give a 16% lower total yield in Lisbon and 23% in Helsinki, respectively.

4.3. *Effect of shading*

The question of possible shading of PV modules deserves attention as the number of hhs in the urban setting considered here is high, or some 10,000 hhs. Previous studies indicate that shading losses could reduce average PV output by 4–7% [25,26] but the instantaneous drop on a module level could be even much higher [27]. In practice is it almost impossible to determine accurately the influence of shading on the PV output as this would necessitate knowing the exact topology of the buildings and the city plan. As the shading effects are worst during low zenith angles, a virtual horizon was used, i.e. the direct solar radiation under 10° solar zenith was cut off, which would lead to a small decrease in the yearly PV

yield. Around noon time when the solar insolation has its maximum and the PV electricity feed into the distribution network is at highest, the effects of the shading will be at minimum due to the high zenith angle. Assuming that most of the PV panels would be on the roofs or on the top floor facades, the effects of the shading on the load and PV matching may therefore remain small.

4.4. Effect of PV penetration levels

The different PV penetration levels cause nonlinear effect in the network. The lowest penetration level, 5% of all the nearly 10,000 hhs having the 1 kW_p PV system (= 50 W_p/hh) caused in all cases positive effects to the network, i.e. smaller network losses. All the generated energy was consumed at local level and the grid only experienced reduced consumption level at daytimes. The second penetration level 50% (= 0.5 kW_p/hh) caused minor current flow to the network making modest voltage rise at some of the network tail sections, but in none of the cases more than 1.007 p.u., which is well within the limits of fluctuations accepted. In the comb-type network no over-voltages (>1.0 p.u.) were observed.

The third case, or 100% (1 kW_p/hh), caused noticeable voltage rises in all the network types. With south-oriented PV panels in tree-type network (Fig. 3a) the voltage went close to the 1.025 p.u. voltage limit, while the comb-type network experienced voltages around 1.01 p.u. When the fourth 200% or 2 kW_p/hh PV penetration level was applied, most of the cases topped the 1.025 p.u. voltage limit except for the comb-type network which remained under 1.020 p.u.. The ''East–West''-orientating case with the looped network also stayed within the voltage limits. When the PV power generation is compared with the induced network losses, the south orientated PV panels with 1 kW_p PV per hh is closest to the optimum.

The key results from the case studies have been collected to Table 3 but excluding the lowest PV cases (not significant effects) and the cases (mainly 2 kW_p/hh) exceeding the voltage limit 1.025 p.u. For comparison, the maximum voltage levels for 2 kW_p/hh representing the worst case are also shown in the last column. In practice, only the comb-type network could absorb the highest PV penetration rate, in other cases half of this could be used when staying within the voltage limits. The 1 kW_p/hh PV use caused negligible voltage rise in the comb case. The highest voltage rise was experienced with tree-type networks.

Feeding PV into the electric network affects not only the voltage but also the losses in the network. The network losses without PV would be 0.65–0.83% of the total load in Helsinki and 0.67–0.94% in Lisbon, respectively. Adding PV up to 1 kWp/hh typically reduces the electric losses, but a 2 kWp/hh level increases the losses in all cases. The losses would be then from 1.5% to 1.9% in Helsinki and 1.6% to 2.2% in Lisbon, respectively, the highest being with a tree-type network. With the 0.5 kW_p/hh level, the losses typically decrease by 20%.

The ''East–West''-orientated PV case with a looped network was also included in Table 3. This case demonstrates that when the 2.5% voltage rise limit was slightly exceeded when the panels were directed to south, the redirection to East–West would reduce the voltage rise and keep it within the limits. This is caused by lower energy production and slightly different hourly distribution, which reduces the mid-day voltage peaks.

Table 3
Summary results from the case studies

Network topology	Load type	Number of hhs	Annual consumption (kWh/hh)	Total PV capacity		Total PV production (% of cons.[a])	Azimuth angle	Energy from grid (% of cons.[a])	PV to grid (% of cons.[a])	Voltage range (p.u.)	Network losses	Maximum voltage for 2 kWp/hh
				kWp/hh	MWp							
Comb	HEL	11232	2324	—	—	0.0	—	100.8	0.0	1.0000–0.9754	0.65	1.0314
Comb	HEL	11232	2324	0.5	5.6	21.7	0°	81.9	3.0	1.0013–0.9754	0.53	1.0314
Comb	HEL	11232	2324	1.0	11.2	43.3	0°	75.6	18.3	1.0132–0.9754	0.64	1.0314
Comb	LIS	9360	2714	—	—	0.00	—	100.7	0.0	1.0000–0.9756	0.67	1.0203
Comb	LIS	9360	2714	1.0	9.4	63.1	0°	59.5	22.1	1.0045–0.9756	0.52	1.0203
Comb	LIS	9360	2714	2.0	18.7	126.2	0°	59.5	81.3	1.0203–0.9756	1.58	1.0203
Comb	LISAG	8424	2906	—	—	0.00	—	100.7	0.0%	1.0000–0.9756	0.65	1.0203
Comb	LISAG	8424	2906	1.0	8.4	58.8	0°	60.4	18.8	1.0039–0.9750	0.48	1.0184
Comb	LISAC	8424	2906	2.0	16.8	117.6	0°	57.1	73.4	1.0184–0.9750	1.33	1.0184
Loops	HEL	9856	2324	—	—	0.0	—	100.8	0.0	1.0000–0.9758	0.76	1.0461
Loops	HEL	9856	2324	0.5	4.9	21.6	0°	82.0	3.0	1.0045–0.9758	0.62	1.0461
Loops	HEL	9856	2324	1.0	9.9	43.3	0°	75.7	18.3	1.0193–0.9758	0.77	1.0461
Loops	LIS	8960	2714	—	—	0.0	—	100.8	0.0	1.0000–0.9754	0.83	1.0330
Loops	LIS	8960	2714	0.5	4.5	31.8	0°	69.4	0.7	1.0000–0.9754	0.55	1.0330
Loops	LIS	8960	2714	1.0	9.0	63.6	0°	59.7	22.6	1.0104–0.9754	0.69	1.0330
Loops	LISAC	8064	2906	—	—	0.0	—	100.8	0.0	1.0000–0.9752	0.81	1.0292
Loops	LISAC	8064	2906	0.5	5.2	29.5	0°	71.3	0.3	1.0000–0.9752	0.55	1.0292
Loops	LISAC	8064	2906	1.0	4.0	59.0	0°	60.6	19.0	1.0090–0.9752	0.63	1.0292
Tree	HEL	12300	2324	—	—	0.0	—	100.8	0.0	1.0000–0.9751	0.83	1.0547
Tree	HEL	12300	2324	0.5	6.2	21.7	0°	82.0	3.1	1.0069–0.9751	0.68	1.0547
Tree	HEL	12300	2324	1.0	12.3	43.5	0°	75.7	18.4	1.0235–0.9751	0.86	1.0547
Tree	LIS	11316	2714	—	—	0.0	—	100.9	0.0	1.0000–0.9757	0.94	1.0400
Tree	LIS	11316	2714	0.5	5.7	31.7	0°	69.6	0.6	1.0006–0.9757	0.62	1.0400
Tree	LIS	11316	2714	1.0	11.3	63.4	0°	59.7	22.4	1.0142–0.9757	0.76	1.0400
Tree	LISAC	10332	2906	—	—	0.0	—	100.9	0.0	1.0000–0.9755	0.91	1.0364
Tree	LISAC	10332	2906	0.5	5.2	29.6	0°	71.3	0.3	1.0004–0.9755	0.62	1.0364
Tree	LISAC	10332	2906	1.0	10.3	59.2		60.6	19.1	1.0127–0.9755	0.69	1.0364
Loops	LISAC	8064	2906	2.0	8.1	98.89	−90°/90°	56.29	53.9	1.0230–0.9752	1.29	1.0230

[a]As percentage from annual consumption.

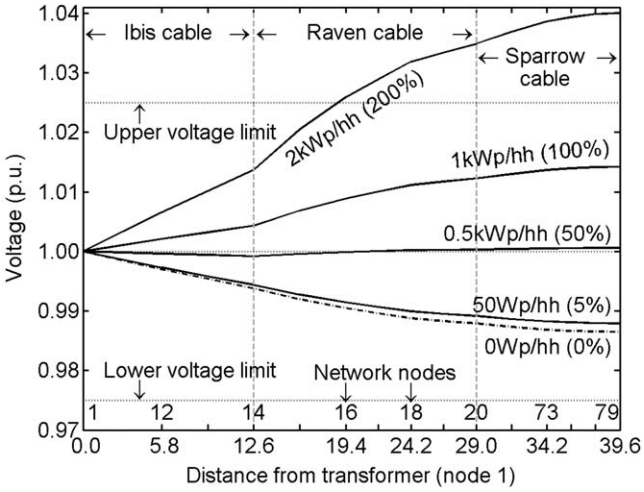

Fig. 9. Example of voltage fluctuation along the electric network for a single hour (noon) in Lisbon with different PV penetration levels.

4.5. Other observations

Transformers connected to medium- and low-voltage distribution networks may also have a significant influence to the ability of the network to accommodate distributed generation. If the transformer cannot dynamically adapt to voltage changes caused by the distributed generation, which is a typical situation with conventional transformers, only a moderate level of variation can be allowed to the distributed PV generation. On the other hand, if a dynamic response in the range of $\pm 2.5\%$ voltage fluctuation is allowed, larger penetration levels are possible, or in our case 100% PV of total load.

It also appears that a single linear network that is strong enough to supply a large amount of hhs is also good for PV-integration. A loop-type network proved to be slightly weaker than the linear comb-network. An individual loop could be extended to a longer distance than an open-ended comb-type network with a significantly stronger cable type. The comb-type network overdid by far the other networks, when it comes to the PV integration, due to the strong main line needed in this type of a network and topological effects. Our observations indicate that the larger the share of the customers that are far away from the supplying transformer (e.g. large tree-type network), the poorer is the network's capability to accommodate PV generation capacity.

In Table 3, the maximum voltage levels in the whole network were shown. In practice the voltage along the line varies, the variation increasing when moving away from the transformer (node 1). In Fig. 9, an example of the voltage variation is shown for Lisbon during 12–13 h on a bright spring day in a tree-type network for all PV penetration levels. Both the adverse and positive effects of PV are clearly demonstrated.

5. Conclusions

The simulation results demonstrated, that high penetration levels of PV power generation may cause voltage problems in the electrical network but also depend on the

network type. The comb-type network showed the best performance. On the other hand all network types studied can handle PV without significant problems both in a northern and southern climate with an amount of PV equaling up to the load (here 1 kW_p/hh, case 100%).

The results also demonstrate that the mismatch between PV production and domestic electricity consumption cannot be fully compensated through orientation of the PV panels. Thus the PV is unable to shave the domestic load peak appearing in our cases in the early evening hours. An east–west orientation of the PV panels reduces, however, the PV peak in the noon by 30% in Helsinki and 10% in Lisbon, respectively.

PV integration into the network influences both the voltage and network losses positively at least up to a 1 kW_p/hh (100% of annual domestic load) when using the voltage design limits. If no increase in voltage from the non-PV case is allowed, the 0.5 kW_p/hh (50%) would be the limit for PV. When going for 2 kW_p/hh (200% of annual load) all but the comb-type networks demonstrate clear over voltage situations. Also, the annual network losses are more than doubled in this case compared to a neutral network without PV.

Acknowledgments

The post graduate grant of Helsinki University of Technology and the grant from TES/Gasum fund that were issued to Jukka Paatero are gratefully acknowledged.

Appendix A. Calculation procedure for a radial network

Step 1: Initial values are given to voltages of network nodes U_k^0 (typically nominal voltage).

Step 2: Network node currents from loads and generation are computed with $J_k^t = P_k^t / U_k^t$ and then summed following Kirchoff's first law [24].

Step 3: Node voltages are computed with $U_k^{t+1} = U_i^{t+1} - Z_k I_k^t$. Here U_i^t is the node from where node U_k^t gets its current.

Step 4: If $\left|U_k^{t+1} - \overline{U_k^t}\right| > \varepsilon$, where ε is the predefined tolerance, the iteration has not converged. Then $t = t + 1$ and go to Step 2.

Step 5: When the iteration has converged, the values U_k^t and J_k^t are the result.

Here, t refers to the computation round and k to the network node number. P_k^t refers to production or consumption in node k. In Step 3, the nodes that have positive total production that give current to other nodes have to be computed first.

Appendix B. Calculation procedure for a looped network

Step 1: When omitting the inductance between network nodes and earth, the current flow for each network node k can be written by Kirchoff's law as

$$J_k = Y_{k0} U_k + \sum_{i=1, i \neq k}^{n} Y_{ki}(U_k - U_i), \tag{B.1}$$

where y_{kj} is the admittance for line between nodes k and I and y_{i0} is the admittance between node k and earth. Eq. (B.1) can be expressed in matrix for as $\mathbf{j} = \mathbf{Yu}$ and reopened as

$$J_k = \sum_{i=1}^{n} Y'_{ki} U_i. \tag{B.2}$$

Step 2: The power flow into any node k is computed as follows:

$$P_k - \hat{j} Q_k = U_k^* J_k = U_k^* \sum_{i=1}^{n} Y'_{ki} U_i. \tag{B.3}$$

Using a polar form for voltage ($U_k = U_k e^{\hat{j}\delta_k}$, $Y'_{ki} = Y'_{ki} e^{-\hat{j}\theta_{ki}}$) Eq. (B.2) can be divided into two separate problems:

$$P_k = \sum_{i=1}^{n} U_k Y'_{ki} U_i \cos(\theta_{ki} - \delta_i + \delta_k), \tag{B.4}$$

$$Q_k = \sum_{i=1}^{n} U_k Y'_{ki} U_i \sin(\theta_{ki} - \delta_i + \delta_k), \quad k = 1, \ldots, n. \tag{B.5}$$

Step 3: The Newton–Raphson method is employed to solve voltage values U_k and phase angles δ. The equation to be solved is of the following form (see also Eq. (1)):

$$\begin{bmatrix} \Delta P_1 \\ \vdots \\ \Delta P_{n-1} \\ \Delta Q_1 \\ \vdots \\ \Delta Q_{n-1} \end{bmatrix} = \begin{bmatrix} & H & & N & \\ & & & & \\ & & & & \\ & M & & L & \\ & & & & \end{bmatrix} \begin{bmatrix} \Delta\delta_1 \\ \vdots \\ \Delta\delta_{n-1} \\ \Delta U_1 \\ \vdots \\ \Delta U_{n-1} \end{bmatrix}, \tag{B.6}$$

where the Jacobean matrices H, N, M, and L are

$$H_{ki} = \frac{\partial P_k}{\partial \delta_i}, \quad N_{ki} = \frac{\partial P_k}{\partial U_i}, \quad M_{ki} = \frac{\partial Q_i}{\partial \delta_j}, \quad L_{ij} = \frac{\partial Q_i}{\partial U_j}. \tag{B.7}$$

Eq. (B.5) is solved iteratively until an adequate precision is achieved. For the next simulation time step, the computation is started from Step 1.

References

[1] Beise M. The international adoption of photovoltaic energy conversion. Int J Energy Technol Policy 2004;2:272–83.

[2] IEA-PVPS. Trends in photovoltaic applications—survey report of selected IEA countries between 1992 and 2003. IEA PVPS T1-13:2004. IEA-PVPS Task 1, 2004.

[3] Green MA. Crystalline and thin-film silicon solar cells: state of the art and future potential. Solar Energy 2003;74:181–92.

[4] van der Zwaan B, Rabl A. Prospects for PV: a learning curve analysis. Solar Energy 2003;74:19–31.

[5] Mermoud A, Roecker C, Bonvin J. PVsyst, version 3.3. Switzerland: 2004. Available online at http://www.pvsyst.com

[6] CETC-Varennes. RETScreen International. Canada: Natural Resources Canada; http://www.retscreen.net/ang/menu.php. Visited 06/07/2005.
[7] Kurosawa K. Energy from the desert: feasibility of very large scale photovoltaic power generation (VLS-PV) systems. London, UK: James & James; 2003.
[8] Hoff T, Shushnar G. Two years of performance data for the world's largest photovoltaic power plant. IEEE Trans Energy Conversion 1987;2:232–5.
[9] Paatero JV, Lund PD. A model for generating household electricity load profiles. Int J Energy Res 2005;30:273–90.
[10] Jenkins N, Allan R, Crossley P, Krischen D, Strbac G. Embedded generation. London: Institution of Electrical Engineers; 2000.
[11] Elovaara J, Laiho Y. Fundamentals in electric engineering. Espoo, Finland: Otatieto; 1999 [in Finnish].
[12] Stott B. Review of load-flow calculation methods. Proc IEEE 1974;62:916–29.
[13] Stott B, Alsaç O. Fast decoupled load flow. IEEE Trans Power Apparatus Systems 1974;93:859–69.
[14] van Amerongen RAM. A general-purpose version of the fast decoupled load flow. IEEE Trans Power Systems 1989;4:760–70.
[15] Duffie JA, Beckman WA. Solar Engineering of Thermal Processes, 2nd ed. New York, USA: Wiley; 1991.
[16] ABB. Technical information and tables, 10th ed. Vaasa, Finland: Ykkös-Offset Ltd.; 2000 [in Finnish].
[17] DGGE-DE. Table "consumption of electric energy per activity sector". Portugal: Direcço Geral de Geologia e Energia, Divisão de Estatística; 2004 [in Portuguese].
[18] UN-DESA. Table A.13. Population of capital cities in 2003. In: World urbanization prospects: the 2003 revision. New York: United Nations, Department of Economic and Social Affairs, Population Division; 2004. p. 274–7.
[19] Sidler O. Demand side management. end-use metering campaign in 400 households of the European Community. SAVE Programme, Project EURECO France: Commission of the European Communities; 2002.
[20] EIU. Executive Briefing: Portugal. Economist Intelligence Unit; http://eb.eiu.com/index.asp?layout=one-click&country_id=1740000174. Visited 5/31/2005.
[21] Pearson R. In: Lower carbon futures. University of Oxford: Environmental Change Institute; 2000.
[22] CEC. Test reference years TRY—weather data sets for computer simulations of solar energy systems and energy consumption in buildings. CEC, DG XII. Brussels, Belgium: Comission of the European Communities; 1985.
[23] SMIS. Russia's Weather Server—Weather Archive—Lisbon, Portugal. Russia, Moskow: Space Research Institute, Space Monitoring Information Support laboratory; http://meteo.infospace.ru/wcarch/html/e_day_stn.sht?num=3668. Visited 5/30/2005.
[24] Alanso M, Finn EJ. Fundamental university physics -v. 2. Fields and waves, 2nd ed. Reading, MA: Addison-Wesley; 1983.
[25] Kovach A, Schmid J. Determination of energy output losses due to shading of building-integrated photovoltaic arrays using a ray-tracing technique. Solar Energy 1996;57:117–24.
[26] Kurokawa K. Realistic values of various parameters for PV system design. Renew Energy 1998;15:157–64.
[27] Alonso-Gracia MC, Ruiz JM, Herrmann W. Computer simulation of shading effects in photovoltaic arrays. Renew Energy 2006, in press, doi:10.1016/j.renene.2005.09.030.